Carbon 206 (2023) 26–36

Contents lists available at ScienceDirect

Carbon

journal homepage: www.elsevier.com/locate/carbon

Compositing graphene oxide with carbon fibers enables improved dynamical thermomechanical behavior of papers produced at a large scale

Krystian Kowiorski [a], Marcin Heljak [b], Agata Strojny-Nędza [a], Bartosz Bucholc [a,c], Marcin Chmielewski [a,d], Małgorzata Djas [e,f], Kamil Kaszyca [a], Rafał Zybała [a,b], Marcin Małek [g], Wojciech Swieszkowski [b], Adrian Chlanda [e,*]

[a] Łukasiewicz Research Network - Institute of Microelectronics and Photonics, Materials for Energy Sector Research Group, Aleja Lotników 32/46, 02-668, Warsaw, Poland
[b] Warsaw University of Technology, Faculty of Materials Science and Engineering, Wołoska 141, 02-507, Warsaw, Poland
[c] Institute of Fundamental Technological Research of the Polish Academy of Sciences, Pawińskiego St. 5B, 02-106, Warsaw, Poland
[d] National Center for Nuclear Research, Materials Research Lab, Świerk, 05-400, Otwock, Poland
[e] Łukasiewicz Research Network - Institute of Microelectronics and Photonics, Flake Graphene Research Group, Aleja Lotników 32/46, 02-668, Warsaw, Poland
[f] Warsaw University of Technology, Faculty of Chemical and Process Engineering, Waryńskiego 1, 00-645, Warsaw, Poland
[g] Military University of Technology, Faculty of Civil Engineering and Geodesy, Research Laboratory of WIG, 2 Gen. S. Kaliskiego St., 00-908, Warsaw, Poland

ARTICLE INFO

Keywords:
Flake graphene
Graphene oxide
Graphene oxide paper
Carbon fibers
Mechanical properties

ABSTRACT

This article discusses the morphology and thermomechanical properties of graphene oxide (GO) paper sheets and GO paper composites reinforced with carbon fibers. GO paper was fabricated using GO paste obtained by the condensation of GO aqueous solution synthesized using the Hummers' method. Carbon fibers were implemented to improve the mechanical properties of the pristine GO paper. All the investigated papers were subjected to thermal treatment to check thermo-related morphological and mechanical properties. The results presented in this study allowed for the deeper insight into morphological, structural, and mechanical volume and surface-related properties of pristine GO and GO-based composite materials reinforced with carbon fibers. We showed that there are two important factors that should be taken into consideration for the design and fabrication of GO-based papers. These factors were the concentration of the reinforcing agent and the thermal reduction of the papers. Both factors have influenced the final properties of the resulting GO-based papers. For the first time, it was revealed how the addition of the reinforcing material affects the GO paper thermal expansion coefficient.

1. Introduction

Carbon materials are widely used in many fields of science and have already been commercialized and implemented in different industries. It is possible because of their unique properties, including electrical and thermal conductivity, low density, and good mechanical properties. In addition, carbon can be produced in different forms, such as fibers, mats, flakes, and tubes. In recent years, scientists have been trying to use thin film or paper-like materials for energy storage devices [1,2] or water storage systems. Such materials are also used to strengthen polymer composites and make them lighter at the same time. They are also desirable because of their low cost in relation to the resulting properties of newly created composite materials.

Apart from carbon in the form of carbon fibers (CFs), flake graphene has recently become a very popular material [3–8]. Graphene is an allotropic form of carbon consisting of a honeycomb network of carbon atoms and is described by its high electrical conductivity and excellent Young's modulus and tensile strength [9,10].

This work focuses on one of graphene's derivatives, which is graphene oxide (GO), formed into paper sheets [11]. GO paper was first received by a group of scientists from Northwestern University (USA) in 2007 from a water suspension of GO [12]. Notably, it is also possible to obtain such graphene-based material from a reduced graphene oxide (rGO) suspension [13]. Such material has unique physical, chemical, mechanical, and optical properties, making it a very promising candidate for countless applications in biomedicine, automotive, aviation, sensors, military, etc. [14–18]. Interestingly, an addition of only a few percent of carbon nanotubes to the rGO suspension significantly

* Corresponding author.
E-mail addresses: adrian.chlanda@gmail.com, adrian.chlanda@imif.lukasiewicz.gov.pl (A. Chlanda).

https://doi.org/10.1016/j.carbon.2023.02.009
Received 13 October 2022; Received in revised form 1 February 2023; Accepted 4 February 2023
Available online 6 February 2023

increased electrochemical properties of the resulting material [19,20]. The most frequent attempts were aimed to produce graphene paper using two approaches: vacuum filtration and casting into molds followed by solvent evaporation. Both methods have limitations, mainly regarding the size of the produced paper, resulting from the size of membranes used in the vacuum filtration technique (usually a few centimeters in diameter), or size of casting of molds [12]. In one of the newest publications, Yao et al. [21] proposed an innovative technique to transform graphene paper into a 3D graphene foam. It was achieved by soaking the graphite paper sheets in liquid nitrogen. The authors successfully implemented this material as a cathode for efficient chromium reduction present in wastewater. Dai et al. [22] have designed a system of vertically aligned graphene monoliths (VAGMs). To fabricate such monoliths, the authors first had to produce a graphene paper with a diameter of 28 cm, which is of similar size as used in our studies (Fig. 1). The authors implemented a vacuum filtration of graphene/ethanol dispersion through a custom-made porous polytetrafluoroethylene (PTFE) membrane, followed by a cold pressing and subsequent thermal treatment. Such VAGM-based material was then tested as a cooling electronic system. The authors concluded that such material can be used for electronic thermal management.

In 2013, an innovative method of obtaining large-format graphene paper was developed and patented ("Method of preparing graphene paper" EP2842910B1) in the Łukasiewicz Research Network – Institute of Microelectronics and Photonics [23]. Most of the previous methods described in the literature did not allow to produce large-area paper sheets. The developed method enables fabrication of large-area paper sheets (with lateral size of ca. 30 × 10 cm) (Fig. 1) and scaling up the whole process to obtain even bigger paper sheets.

Simultaneously, it should be underlined that the thermal properties of as-synthesized GO flakes are well established and described in the scientific literature [24,25]. At the same time, we want to point out that after the elimination of oxygen-based functional groups (after the reduction), the thermal properties of rGO flakes are going to be better than GO flakes [26]. Having in mind that the GO paper fabricated in this study is composed in a straightforward manner from GO flakes (without any thermal/chemical/light treatment), we hypothesize that it is characterized by similar properties as pristine GO flakes.

In this work, we present the results of morphological and thermal-related examination of GO paper and GO paper composite reinforced with two concentrations of CFs: 0.3% and 3% w/w. Furthermore, we examined the *in situ* dynamical mechanical properties as a function of temperature. It was reported that an increment of vacancy defects present in the structure of the material was followed by the alteration of the number of functional groups. This was further translated to mean that the regulation of thermal conductivity of GO can be carried out by tuning of functional groups' concentration. Contrary to the literature reports [10,27,28], GO paper made of GO flakes has low mechanical strength. For this reason, an attempt to produce GO paper composite with the addition of CF was made. Such fibers are commonly used as a reinforcing material, similar to polymeric fibers [29,30]. The CF consists almost exclusively of expanded carbon structures chemically similar to graphite, which makes them nonflammable and resistant to chemicals.

Fig. 1. Image of GO paper fabricated in this study. (A colour version of this figure can be viewed online.)

The novelty of the presented work is combined with several aspects. First, in this article, we described an efficient and feasible technique for the production of large-scale GO paper. Moreover, we showed that based on the pristine GO paper, it is also possible to fabricate the composite material with bolstered mechanical properties. Finally, we have presented a multitechnique approach for the detailed description of morphology and thermomechanical properties of the resulting material, including *in situ* examination of this material's feature.

Taken together, all the results presented in this article can be implemented by other scientific teams and companies looking for attractive, mechanically stable, and functional materials with the ability of effective heat absorption.

2. Materials and methods

2.1. Synthesis of GO

GO flakes and GO papers (G-Flake®) have been fabricated at the Łukasiewicz Research Network – Institute of Microelectronics and Photonics. The first stage for the production of GO paper was the synthesis of GO flakes. The modified Hummers' method was used for this purpose [27,31]. In brief, graphite flakes with diameter ranging from 120 to 150 μm (Asbury Carbons, USA) were placed in a reactor (Radleys-Reactor-ReadyTM Great Britain) containing a concentrated mixture of sulfuric acid (H_2SO_4, Chempur, Poland). Subsequently, potassium permanganate ($KMnO_4$, Chempur, Poland) and potassium nitrate (KNO_3 Chempur, Poland) were added to the mixture. The oxidation process was performed for several hours and eventually stopped by the addition of deionized water and hydrogen peroxide (30% H_2O_2, Chempur, Poland). To achieve homogeneous dispersion of GO flakes in water, the purification and exfoliation processes were also performed. The concentration of the resulting aqueous suspensions of GO was ca. 4 g/l and the average flake size was ca. 11 μm.

2.2. GO paper preparation

GO suspension obtained in Section 2.1 was later concentrated to ca. 15 g/l to produce GO paper sheets. For this purpose, a centrifuge (Thermo Lynx 4000, Osteorode, Germany) set to 10,000 rpm operated for 1 h. The subsequent concentrated solution was further concentrated at 40 °C using a magnetic stirrer for about 170 h. The GO paper was obtained according to the procedure of the patent entitled "Method of preparing graphene paper" EP2842910B1 method developed at the Łukasiewicz Research Network – Institute of Microelectronics and Photonics [23] (Fig. 2). The aforementioned method involved spreading concentrated GO suspension between two flexible porous substrates.

Next, substrates with applied GO suspension were squeezed between two rollers. Finally, substrates were left to dry for about 24 h at room temperature (RT). After drying, the substrates were removed, leaving ready GO paper sheets.

2.3. Modification of GO paper with CFs

CFs were implemented to strengthen the mechanical properties of GO paper in elevated temperatures related to the actual operating conditions of the GO paper. The fibers (about 5 μm in diameter) were mechanically separated from commercially available mats (Composite Technologies, Poland). The modification of GO paper was carried out by the addition of 0.3% and 3% w/w of CFs to the GO paste. A noncontact mixer (FlackTek, SpeedMixer, USA) was used as a mixing device to prepare composite GO papers. Mixing took place at RT for 5 min at the speed of 3000 rpm.

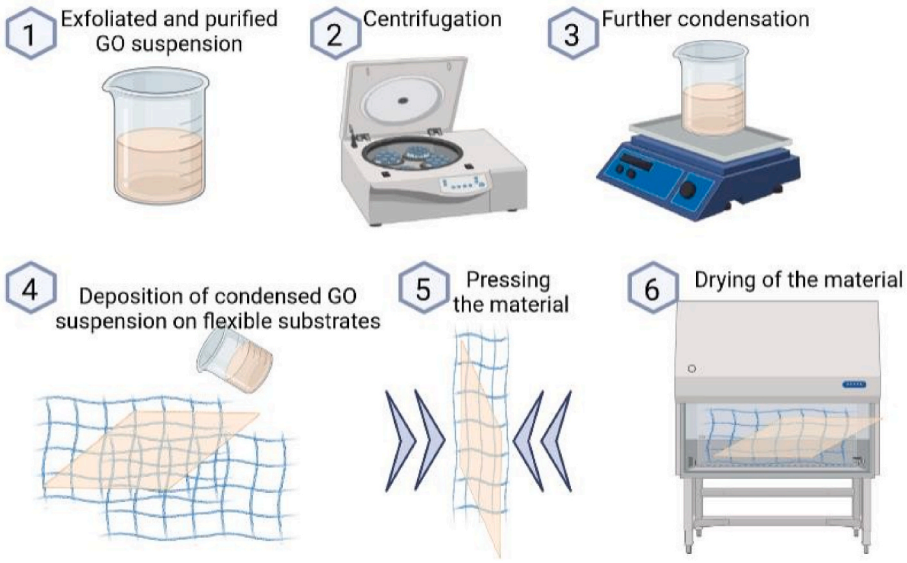

Fig. 2. Schematic illustration of GO paper fabrication. Composed with BioRender [32]. (A colour version of this figure can be viewed online.)

This protocol enabled the preparation of three types of samples, designed as GO_p (pristine GO paper), GO + 0.3%CF (GO composite paper with addition of 0.3% w/w of CF), and GO + 3% CF (GO composite paper with addition of 3% w/w of CF). The amount of CF used in this study was chosen based on the authors' experience with carbon-based composites.

2.4. Thermal treatment of the GO papers

To simulate actual operating conditions of the paper – precisely recreated using thermogravimetry (TG), differential scanning calorimetry (DSC) (Section 2.9), and dynamic mechanical analysis (DMA) (Section 2.10) – some population of the fabricated samples was additionally subjected to thermal treatment (3 h) at 200 °C using the universal oven Memmert UF 55.

2.5. Atomic force microscopy: surface visualization and roughness analysis

Surface visualization of pristine and composite GO-based papers was conducted using the ICON (Bruker) atomic force microscope (AFM) connected to the Nanoscope V controller. GO papers were fixed directly on the table of the microscope. High-resolution topographical and phase-contrast images were registered using a sharp silicon AC200TS scanning probe (Olympus). To ensure stable experimental conditions, the apparatus was closed in a chamber provided by the microscope's manufacturer. Auto-tune procedure was implemented to evaluate the drive frequency of the scanning probe (ca. 146 kHz). Topographical data were registered using tapping-mode (TM) in air with ambient conditions (temperature of ca. 19 °C and relative air humidity of 28%). Roughness analysis was performed based on the registered topographical maps. For this purpose, a freeware software (Gwyddion, ver. 2.56) was implemented. The same experimental setup was used for the estimation of the thickness of G-Flake® GO flakes.

2.6. AFM: stiffness analysis

Analysis of the local (micro- and nanoscaled) alteration of mechanical properties (stiffness) of the surface of tested films was estimated using ICON (Bruker) AFM. The microscope was operating in Quantitative NanoMechanics (QNM) mode. Prior to mechanical data acquisition, experimental setup was calibrated using calibration standards (of known stiffness) provided by the producer of the microscope. We used the AC200TS scanning probe (Olympus) characterized by spring constant of ca. 24 N/m. Recorded stiffness maps were used for further qualitative and quantitative analyses of surface-related mechanical properties. It is worth mentioning that each pixel on the stiffness map is related to the so-called force–distance (FD) curve, from which a material's surface stiffness can be extracted. Raw FD curves were fit to the Derjaguin–Muller–Toporov (DMT) contact mechanic model. The analysis was performed using the Nanoscope Analysis (ver. 1.90) software provided by the microscope's producer.

2.6.1. Scanning electron microscopy: GO flakes, GO paper, and GO paper composite

Auriga (Zeiss) scanning electron microscope (SEM) with a detector (0.5 kV) was used for GO flakes visualization and size estimation. The GO sample was applied from an aqueous solution on a silicon plate (previously immersed in the Piranha solution and dried with compressed air). Then, it was dried at 40 °C for 24 h.

The visualization of the surface of GO paper and the composite paper with addition of CFs was performed using Phenom ProX (FEI) with the backscattered electron mode and 10 kV acceleration voltage. A 0.25 cm^2 square sample was cut from each GO paper. The sample was then mounted on a SEM pin table. Because the material was dried earlier, there was no need for additional drying. The paper itself does not need coating with a conductive agent, and thus this step was omitted.

2.7. Elemental analysis

Elemental analysis was performed using combustion analyzers: CHN628 and OH836 (Leco). The CHN628 analyzer was used for the detection of carbon, whereas the OH836 analyzer was used for the estimation of oxygen in a helium atmosphere. Prior to examination, apparatuses were calibrated with reference samples delivered by the analyzers' producer – in case of CHN628 analyzer, two calibration samples with a strictly defined content of specified elements were used, namely EDTA (composed of 41.09 ± 0.23% carbon) and BBOT (containing 72.42 ± 0.48% carbon). A second analyzer was calibrated with two standards: silicon dioxide and iron (III) oxide, both with a strictly defined compartment of oxygen: 53.05 ± 0.5% in case of silicon dioxide and 30.02 ± 0.4% for iron (III) oxide, respectively. As experimental protocol requires small masses of samples, 0.005 g and 0.01 g microbalance (Sartorius Quintix) was used to determine the weight of the

samples. The examination temperature was set to 950 °C.

2.8. Thermal analysis (DSC/TG)

Thermal analysis (STA) involved the simultaneous use of two research techniques: TG and DSC. It was possible because the conditions during the measurements were identical for the TG and DSC signals. The use of this method increases work efficiency. The thermal decomposition behavior of the samples was analyzed using scanning calorimetry (DSC/TG) (STA 449 F5 Jupiter NETZSCH Company) to determine the decomposition temperature and weight loss during reduction. Measurement was performed in air with a heating rate of 1 °C/min.

2.9. Mechanical properties (DMA)

The tensile properties of the GO papers were determined using Q800 (TA Instruments, USA).

DMA instrument equipped with tension clamps. All static tests aiming to identify the tensile modulus, the ultimate tensile (UTC strength, UTS), and the strain at fracture were performed in the controlled-force mode with a preload of 0.01 N, and the force was applied with a force ramp rate of 2 N/min [33,34]. The tensile modulus was calculated in the initial quasi-linear range of the obtained stress–strain curves (up to 0.1% of strain). To identify the viscoelastic properties' evolution during heat treatment of the GO paper, the temperature sweep test was carried out with a sample displacement amplitude of 5 μm at a temperature range from RT to 250 °C (T_0). The whole test was composed of two thermomechanical cycles. Each of the specimens was heated up to the temperature of 250 °C. Once it was achieved, the specimen was cooled at RT. The cooling stage parameters were not recorded. Obtained data were used to calculate the storage modulus *E*', the loss modulus *E*", as well as the coefficient of thermal expansion (CTE) of the paper-like GO sheets. All the specimens were preloaded to 0.01 N. The CTE was calculated according to the following formula (Eq. (1)):

$$TEC = \frac{(l(T) - l0(T0))/l0(T0)}{\Delta T} \quad (1)$$

where l(T) and $l_0(T_0)$ are the lengths of sample at temperatures T and T_0.

3. Results and discussion

Prior to the examination of the GO papers, we characterized the synthesized GO flakes (G-Flake®). A detailed description of the synthesized material and its stability was described in one of our previous articles [8]. Here, we report only some selected yet vital parameters of the obtained 2D carbon material.

SEM examination was implemented to visualize the as-synthesized GO flakes and measure their average size (Fig. 3), which was estimated at 11.84 ± 4.06 μm. The size of the flakes is much smaller than the size of graphitic precursor – this was related to a multistep synthesis and purification protocol. Notably, using different protocols, it is possible to obtain GO flakes characterized by bigger lateral sizes from the same precursor. The CFs introduced to the GO sheets were described by the diameter of ca. 5 μm (Fig. 4).

AFM examination was done to check the thickness of individual flakes. We have established that most of the flakes examined were characterized by a thickness of ca. 1.26 ± 0.14 nm, revealing almost complete exfoliation of the material.

SEM technique was also used to register cross-sectional images of the GO paper sheets in the initial state as well as paper sheets that underwent thermal treatment (1 h at 200 °C) (Fig. 5). It can be observed that

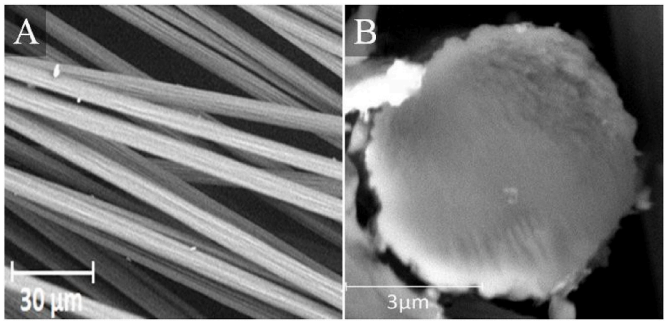

Fig. 4. SEM images depicting (A) carbon fibers introduced into GO paper and (B) cross-section of an individual carbon fiber. (A colour version of this figure can be viewed online.)

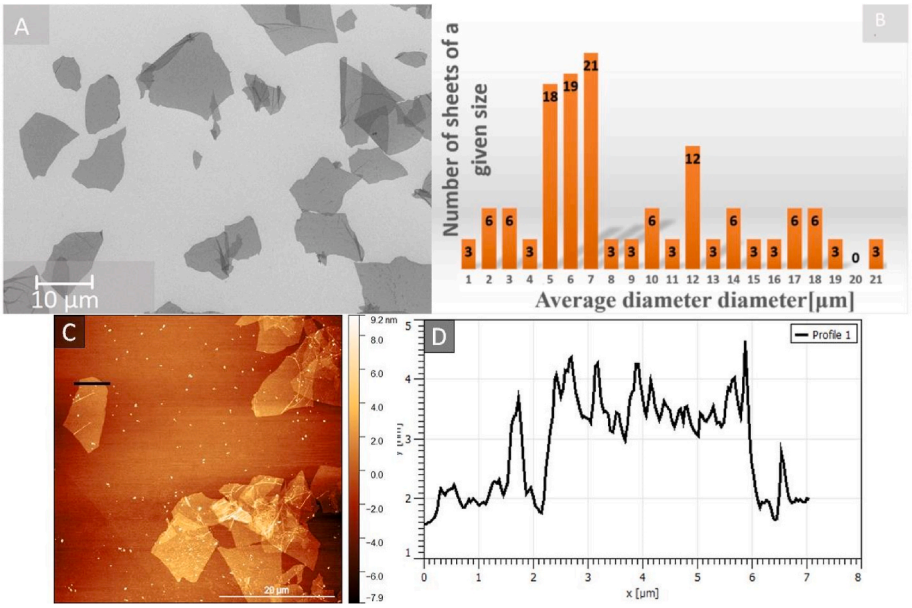

Fig. 3. Morphological analysis of synthesized GO flakes. (A) Representative SEM image of GO flakes after exfoliation and purification. (B) Histogram showing the diameter of GO flakes. (C) Representative AFM topographical map of GO flakes along with the (D) thickness of the selected GO flake. (A colour version of this figure can be viewed online.)

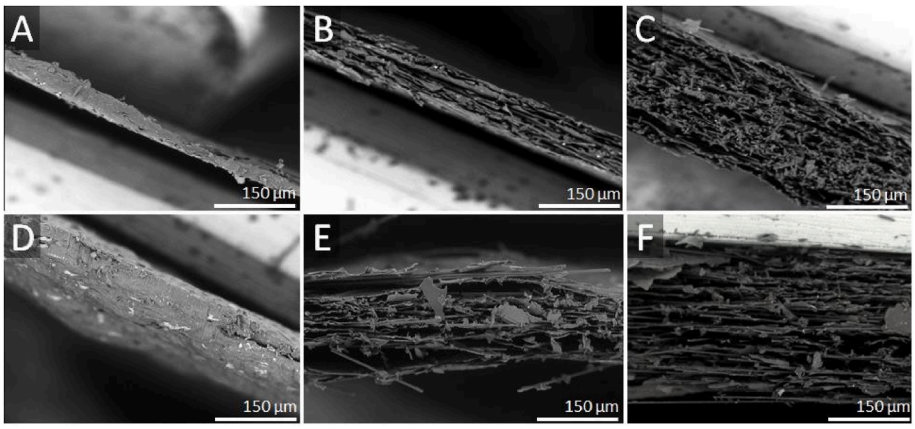

Fig. 5. SEM images of GO paper in the initial state: (A) GO_p; (B) GO + 0.3% CF; (C) GO + 3% CF; (D) GO_p 200 °C; (E) GO + 0.3% CF 200 °C; (F) GO + 3% C F 200 °C. (A colour version of this figure can be viewed online.)

regardless of its composition GO paper in the initial state was made of multiple individual sheets superimposed on each other.

The thickness of the GO paper (established based on Fig. 5) was ca. 49.39 ± 7.19 µm. Individual sheets were separated from each other with air pockets; thus, the cross-sectional architecture of the GO paper resembled a layered sandwich-like structure. Interestingly, the thickness of the pristine GO paper increased after the addition of CF. We observed a fiber-dependent relation: the higher the amount of CF, the thicker the paper: 102.96 ± 3.45 µm (GO + 0.3% CF) and 248.38 ± 14.51 µm (GO + 3% CF). In case of a graphene oxide paper (Fig. 5A) with no additives and with 0.3% additives (Fig. 5B), the structure appears uniform. However, the addition of 3% (Fig. 5C) of CF caused a clear delamination, which, in contrast, did not cause permanent decomposition of the composite paper. We want to underline that the composite paper sheets were mechanically stable and flexible. The mechanical properties of the materials were additionally checked and are described later. Presumably this phenomenon was related to bigger air pockets present in the paper's structure. Bigger air pockets resulted straightforwardly from CF addition as they were located between individual paper sheets. We were not able to obtain appropriate adhesion of GO sheets to the fibrous matrix. Further efforts are needed to functionalize GO sheets of CF to ensure better materials' cohesion. GO papers annealed at 200 °C preserved the aforementioned fiber-dependent trend regarding the materials' thickness. However, the thickness of each material subjected to thermal treatment was higher in relation to its nonannealed *alter ego*: 175.95 ± 12.68 µm (GO_p), 225.50 ± 10.95 µm (GO + 0.3% CF), 384.13 ± 10.35 µm (GO + 3% CF).

An elemental analysis of pristine GO paper and GO paper composites with CF was carried out to analyze the materials' chemical composition, particularly toward the carbon and oxygen content, as these are the most important elements defining graphene-based material *per se* (Table 1). In addition, carbon-to-oxygen ratio is a universal indicator of GO reduction.

By comparing the data gathered in Table 1, it can be concluded that materials deprived of thermal treatment were described with a similar chemical composition with respect to CF additives. Composite papers were characterized by a higher carbon content in relation to GO_p, particularly in the case of GO + 3% CF. Annealing at 200 °C resulted in the reduction of GO papers, which was reflected in the carbon-to-oxygen ratio. Once again, the highest amount of carbon was registered for GO + 3% CF annealed at 200 °C.

Table 1
Results of the combustion elemental analysis of GO flakes and GO papers.

Material	Carbon %	Oxygen %
GO flakes (G-flake)	40.5 ± 0.4	54.9 ± 0.6
G0_p	43.1 ± 0.3	52.2 ± 0.6
GO + 0.3% CF	43.3 ± 0.4	51.6 ± 0.5
GO + 3% CF	48.0 ± 0.4	45.2 ± 0.5
G0_p annealed at 200°C	55.3 ± 0.6	45.4 ± 0.2
GO + 0.3%CF annealed at 200°C	56.7 ± 0.4	45.5 ± 0.3
GO + 3%CF annealed at 200°C	66.2 ± 0.5	36.0 ± 0.3

AFM working in TM was used to register topographical maps (Fig. 6D–F) of three samples, namely GO_p, GO + 0.3% CF, and GO + 3% CF in the initial state (deprived of thermal treatment). The obtained results were used for qualitative and quantitative analyses of the surface of tested materials. Regardless of the type of the tested material, topographical images revealed material-specific information. It was possible to spot additional wrinkles at the surface, which were presumably related to the addition of CF. This assumption was reflected in the average roughness of the surface of GO papers, which increased after incorporation of the fibers. Ra parameter registered for pristine GO was 42.38 nm ± 5.44 nm, whereas for composite papers, the average roughness was 88.09 nm ± 28.44 nm (GO + 0.3% CF) and 144.56 nm ± 58.44 nm (GO + 3% CF). High standard deviation of the presented results (in case of composite papers) is also related to the presence of CF near the surface of the GO sheets. To further investigate the composition of the GO papers, we decided to take advantage of TM capabilities to acquire AFM phase-contrast images. Phase-contrast imaging is a powerful tool for the visualization of the internal structure of materials, which can be helpful in the analysis of chemical composition and surface-related properties of the material, including *inter alia* surface stiffness, adhesion forces, its deformation, or chemical composition [35, 36]. It is particularly useful for the recognition of different phases (materials) in composites. In terms of this study, we implemented this mode to visualize CF located near the surface of the GO sheets. We were able to detect a biphasic composition of the composite materials. Bright areas corresponded to the CF location, whereas dark regions (Fig. 6 B–C) are related to the GO-based matrix. Interestingly, irrespective of CF concentration, the fibers were chaotically distributed within the GO matrix. No privileged direction of their distribution was registered. As expected, the pristine GO paper was characterized by homogeneous structure, and no additional phase was registered (Fig. 6 A).

The same experiment was repeated after annealing of the samples at 200 °C for 3 h. By doing this, we wanted to simulate the conditions of thermal treatment applied to GO papers during the thermomechanical examination. With this approach, we were able to detect subtle micro- and nanoscaled alterations of the surface of the tested samples (Figs. 7 and 8). It was interesting to note that after the aforementioned thermal treatment the surface of the three types of tested materials changed in relation to the initial state. A similar trend regarding average roughness was registered, but still composite papers were characterized by higher roughness (84.12 nm ± 22.44 nm in case of GO + 0.3% CF and 91.31 nm

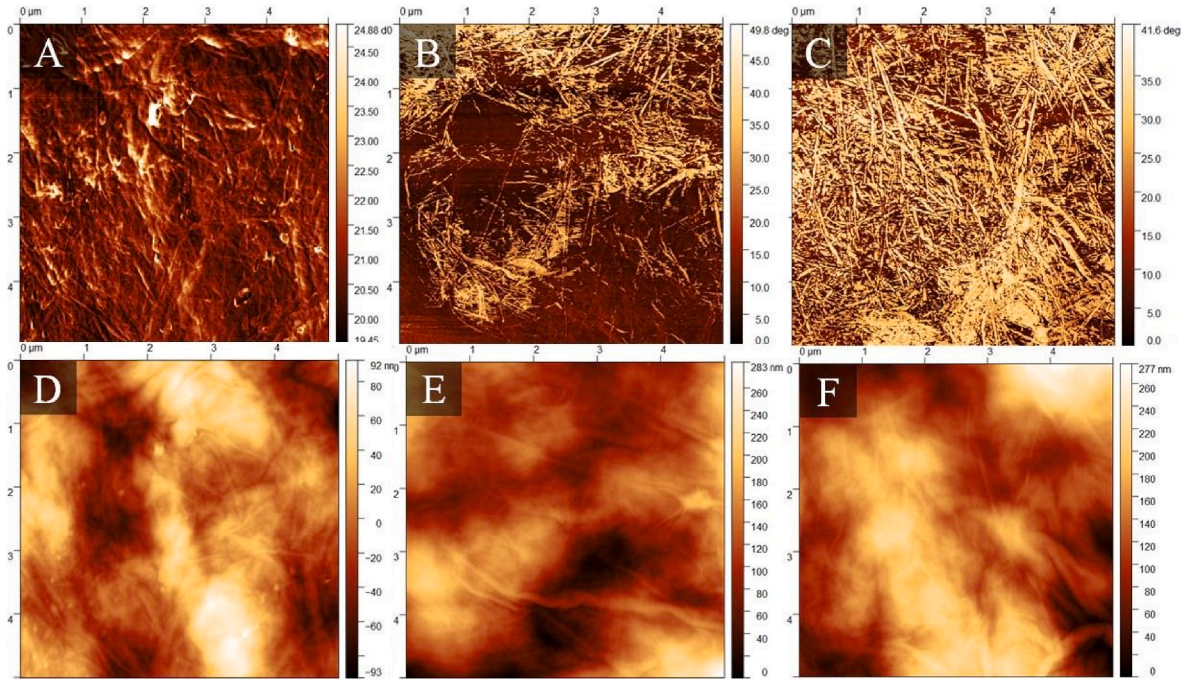

Fig. 6. AFM phase images (A–C) and corresponding topographical images (D–F) of GO_p (A, D), GO + 0.3% CF (B, E), and GO + 3% CF (C, F). Materials tested in the initial state were deprived of thermal treatment. (A colour version of this figure can be viewed online.)

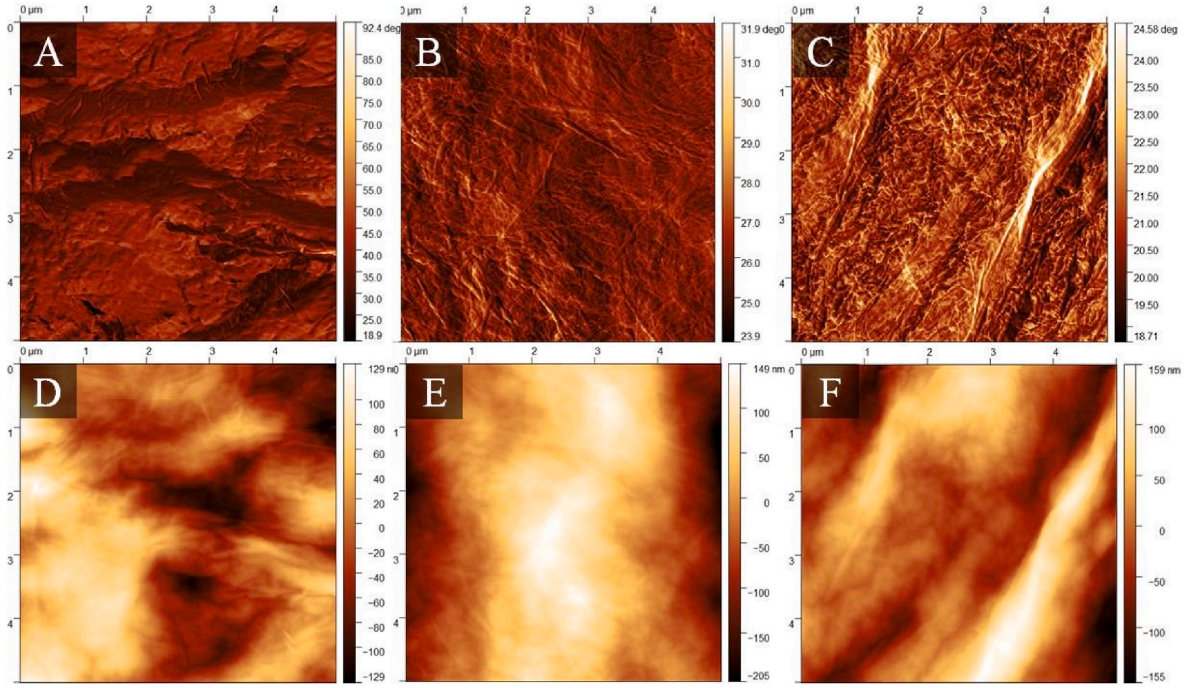

Fig. 7. AFM phase images (A–C) and corresponding topographical images (D–F) of GO_p (A, D), GO + 0.3% CF (B, E), and GO + 3% CF (C, F). Material tested after thermal treatment. (A colour version of this figure can be viewed online.)

± 30.65 nm in case of GO + 3% CF) than in the case of the pristine paper (34.23 nm ± 6.87 nm); however, the differences in Ra parameter between the annealed samples were much smaller. This phenomenon can be attributed to the thermal reduction of the material, which was followed by the elimination of the oxygen-based functional groups. It is worth noting that a similar phenomenon was described by Ramamoorthy et al. [37], who examined the paper made of pristine GO. The authors stated that this is a consequence of release of oxygen-related functional groups from the surface of GO paper sheets; thus, it is an indirect proof of GO reduction. Moreover, in the previously summoned article [37], the authors claimed that the thermally treated paper was characterized by good electrical conductance, whereas the GO paper deprived of thermal treatments was described as an insulator. In another article [38], it was concluded that a GO paper exposed to reduction can be considered as a material for potential application in supercapacitors or high-current applications. This assumption was governed by the

enhanced crystalline structure of rGO paper in relation to pristine GO paper. Such improvement in the structure of the material was also reflected in bolstered Joule heating conductivity. In case of our studies, we have also confirmed the reduction of the annealed material using combustion elemental analysis.

Of special interest was the fact that data recorded on phase-contrast maps were altered in comparison with those recorded for the initial state. CFs, even though visible on both topographical and phase-contrast maps, were much less pronounced. We were not able to record a biphasic structure of the composite papers after annealing, which could be an indirect evidence of GO reduction. It should be underlined that GO (regardless of its form: powder, water solution, or paper sheets) can be easily reduced using different approaches, including but not limited to chemical agents [39], exposition to light [40], or thermal treatment [41]. Regarding the last of the summoned reducing factors, it was proven that a temperature of ca. 50° Celsius is enough to trigger GO reduction [42]. This condition was satisfied in this study. Going back to the merit, we were not able to detect the biphasic structure as after reduction GO was transferred into rGO – a reduced version of GO – which is characterized by a higher amount of carbon in relation to GO. Hence, CFs covered by reduced rGO paper sheets (characterized by higher amount of carbon in relation to papers deprived of thermal treatment) were not recognized as a distinct phase. In order to further justify this conclusion, an elemental analysis was performed to verify carbon and oxygen content of all the tested samples (Table 1).

For all samples, changes in the TG curve associated with weight loss were observed, which corresponded to the peak on the DSC curve (Fig. 8). On the DSC curve, an exothermic peak is observed for all tested materials and its maxima are respectively 193 °C for GO_p, at 197 °C for GO + 0.3% CF, and 198 °C for GO + 3% CF. This peak comes from the decomposition of GO, which is confirmed by the authors [43]. As the DSC curve has a downward trend from the beginning, it is difficult to determine the beginning of this transition, the so-called "onset." The highest weight loss was observed for the pristine GO paper, and it amounts to ca. 22% in the temperature range 150–200 °C, 17% for the GO + 0.3% CF sample, and 10% for GO + 3% CF. This weight loss registered with DSC/TG was related to the thermal decomposition of GO [43]. For the first two samples, that is, GO_p and GO + 0.3% CF, a significant weight loss was also observed in the temperature range of 50–150 °C, which amounts to 26% and 14%, respectively. This weight loss may be due to a possible release of moisture and carbon reduction (combustion).

A comprehensive thermomechanical analysis of the investigated GO paper sheets was carried out. In Fig. 9, results of the thermomechanical analysis are presented. The evolution of the storage modulus, the loss modulus, and the change of the specimen length ($\Delta l/l_0$) is given in the normalized form to facilitate the comparison of the recorded waveforms. All the considered quantities were normalized to initial values recorded at RT (before the first thermomechanical cycle starts). One can see that all the recorded waveforms were subjected to rapid change above the temperature of 150 °C. Based on [44], one can ascribe this phenomenon to the reduction of GO. In the mentioned work, the reduction of GO was manifested as an exothermic event in the DSC analysis at 163 °C – observed only in the first DSC cycle. All the obtained thermomechanical events corresponded to recorded DSC and TGA curves (Fig. 8), which can be taken as the confirmation of the GO reduction occurrence. In case of the recorded DMA profiles, the considered features were no longer observed in the second thermomechanical cycle either. The obtained DMA profiles indicated that the decomposition of GO was associated with a significant decrease of modulus. The recent phenomenon could be explained by the fact that the GO reduction is usually associated with a substantial decrease in the mass of the heated sample [43]. It was revealed that in case of specimens containing 3% CFs the GO decomposition took place at higher temperature than in the case of the pristine GO paper or specimens having a 0.3% content of CFs.

It is worth mentioning that all the investigated materials were characterized by the negative thermal expansion coefficient. This specific property of the GO paper was first reported in Ref. [31]. The values of the thermal expansion coefficient measured in our study were of the same order of magnitude as those reported in Ref. [43]. The CTE of the pristine GO paper was significantly greater than that in the case of composite specimens containing CFs. The latter were characterized by CTE comparable to those measured for the pristine GO paper during the second thermomechanical cycle (Fig. 10D). The values of CTE provided in Fig. 10D were measured within the temperature range preceding the point ascribed to the GO decomposition.

Static tensile tests aiming to identify the tensile modulus, the UTS, and the strain at break were carried out. In Fig. 10 (A, B, and C), the comparison of the tensile test results is presented. One can see that GO + 3% CF samples were the stiffest ones among all the tested samples; however, after the heat treatment, its tensile modulus, as well as UTS, was significantly reduced. Hence, based on elemental analysis results provided in Table 1, it can be concluded that because of the good thermal conductivity of CF incorporated into the GO paper, the reduction of the material was related to the presence of CF. Moreover, it was a CF amount-dependent phenomenon: the higher the concentration of CF, the more efficient the reduction.

GO + 0.3% CF is the only group characterized by an increase in modulus as a result of heat treatment. It was revealed that in the case of GO + 0.3% CF samples the heat treatment had a marginal effect on UTS. The graph presented in Fig. 10C provides evidence that any addition of CF significantly reduced the strain at break.

The thermomechanical examination described in this paper aimed to verify whether or not the GO paper sheet annealing was followed by a change of bulk mechanical properties and how, if any, did the addition of CFs affect these properties. At the same time, we decided to investigate the surface-related mechanical properties of pristine and composite paper sheets using the QNM technique (AFM-based technique). It should be noted that apart from high-resolution imaging of the surface of different materials, the AFM technique enables recording and further quantification of stiffness maps at micro- and nanoscale levels; thus, with this approach, it is possible to address even subtle surface-related

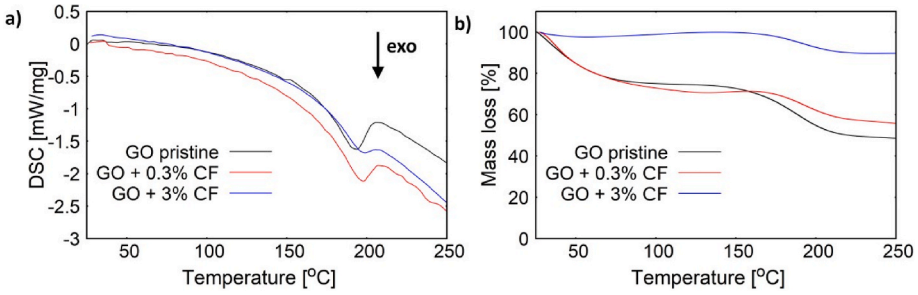

Fig. 8. Thermogravimetric analysis of different types of the graphene oxide paper: (a) DSC curves; (b) TG curves. . (A colour version of this figure can be viewed online.)

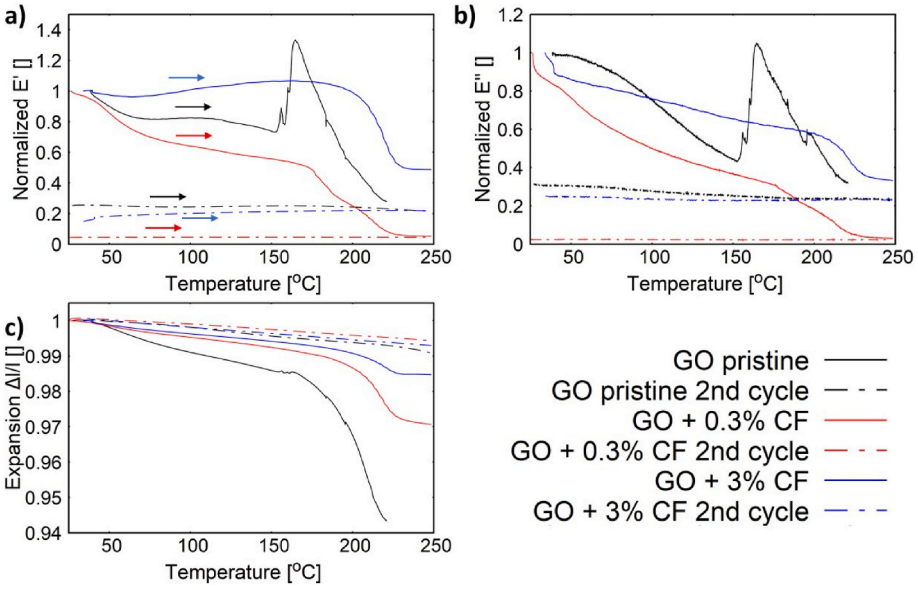

Fig. 9. Dynamic mechanical analysis of the investigated types of GO paper: (a) normalized storage modulus *E*' (arrows indicate the direction of the process); (b) normalized loss modulus *E*''; (c) thermal expansion curves of the investigated types of GO paper ($n = 3$). (A colour version of this figure can be viewed online.)

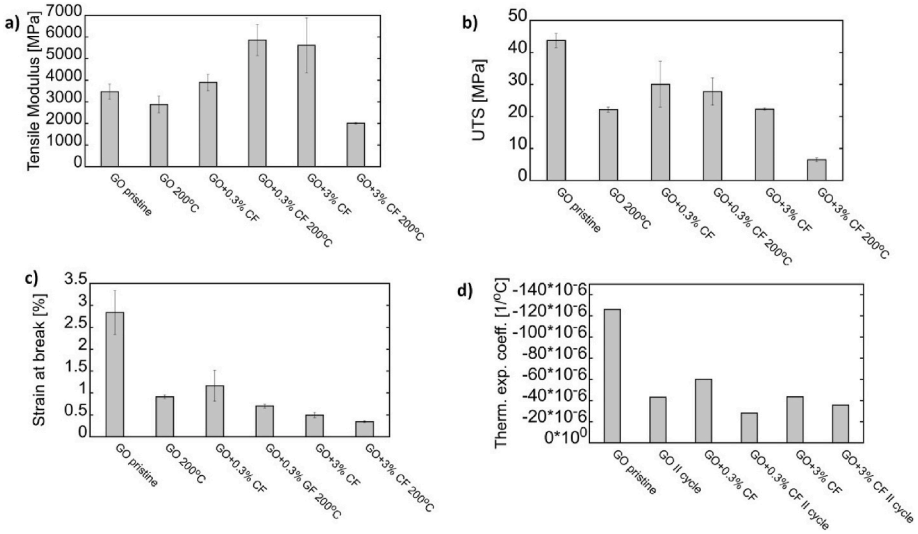

Fig. 10. Comparison of mechanical properties of different types of the graphene oxide paper: (a) tensile modulus; (b) ultimate tensile stress (UTS); (c) strain at break; (d) coefficient of thermal expansion (CTE). (A colour version of this figure can be viewed online.)

changes of mechanical properties of the tested material [45,46]. In order to proceed with this experiment, GO paper sheets (pristine and composites) were tested in two conditions: in the initial state (samples deprived of thermal treatment) and after annealing at 200 °C. To better understand whether alterations in the mechanical properties of GO papers should exclusively be related to their volume, a surface stiffness examination was carried out. We did this because the surface of the material is known to play a crucial role in thermo-related phenomena [47,48]. Thus, it is of utmost importance to look at and describe a surface-related thermomechanical occurrence.

AFM QNM data showed a similar trend in comparison with the bulk mechanical properties. The addition of CF resulted in a higher stiffness of the surface of GO composite paper sheets in relation to the pristine GO paper (Fig. 11). CFs located near the surface of the composite papers were thus responsible for higher DMT modulus values. An interesting phenomenon occurred after thermal annealing of all of the samples. In case of GO_p, we were able to record a bimodal distribution of the DMT modulus value (Fig. 11D). The main contribution to this histogram was similar to the case of GO_p sample in the initial state; however, an additional peak on the histogram (related to more compliant areas of the GO_p surface) was registered. This is direct evidence that the GO paper alone subjected to thermal treatment could lose its integrity and be less mechanically stable; thus, the addition of a stiffer phase (i.e., CF) could be of utmost importance to preserve the stability and durability of GO sheets. Data recorded for composite papers subjected to thermal treatment were free of this additional peak; thus, it was hypothesized that the presence of CF hindered thermal decomposition of the GO paper. Last but not least, the conclusion that was drawn based on the AFM QNM examination of the GO-based papers was that the DMT values were smaller than the values obtained using the DMA technique. This can be easily explained by the differences related to the working principle of these two techniques. As stated earlier, AFM is a surface-related technique, whereas DMA is a volume-related technique; thus, different phenomena and scales are taken into account. Nonetheless, we were

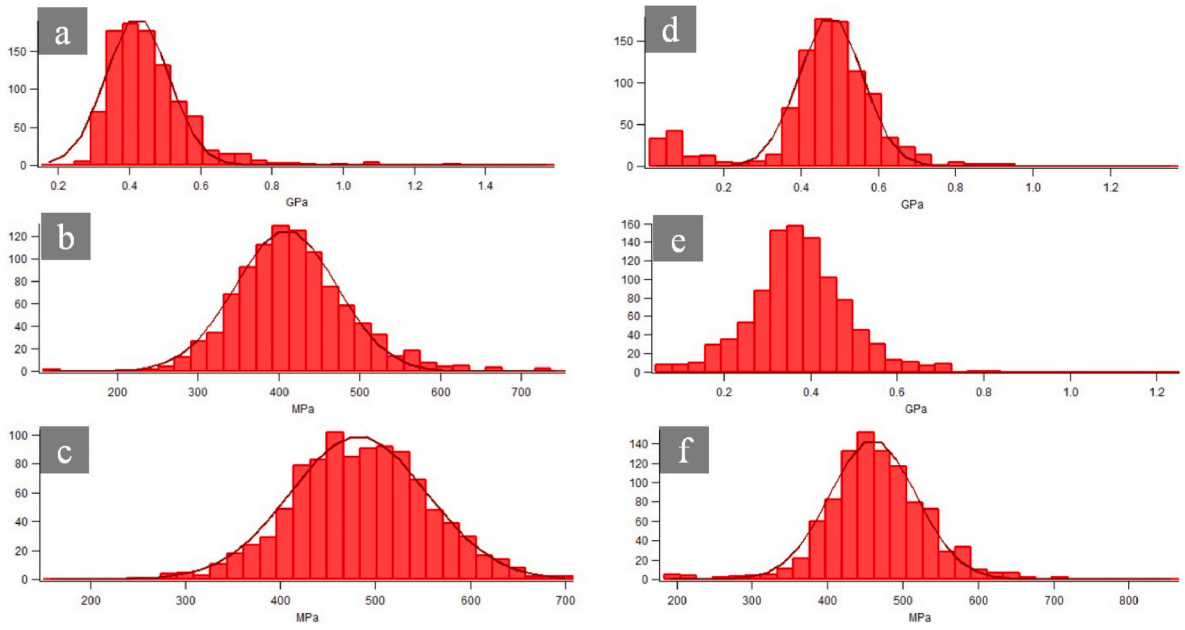

Fig. 11. AFM QNM stiffness maps (A–F) and corresponding histograms of DMT modulus value (a–f) of GO_p (A, D, a, d), GO + 0.3% CF (B, E, b, e), GO + 3% CF (C, F, c, f). A–C (and a–c) show data recorded for materials deprived of thermal treatment, whereas D–F (and d–f) show data recorded for materials annealed at 200 °C. The y scale is the number of the collected force– distance curves fitted (with the DMT model) to the designated stiffness value. (A colour version of this figure can be viewed online.)

able to prove that both presented techniques enabled a deeper insight into the thermo-related mechanical properties of the GO-based paper sheets, and moreover, both techniques generated similar results in terms of CF concentration and thermal treatment of the tested materials.

4. Conclusions

The aim of this study was to describe thermomechanical, structural, and morphological features of pristine GO paper, along with composite GO papers reinforced with CFs. As such, we want to underline that, to the best of our knowledge, this is the very first article to describe the aforementioned examination of composite GO-based paper sheets. In addition this is the first study in which the DMA examination of bulk mechanical properties of GO-based papers was followed by AFM evaluation of the mechanical properties of the surface of the tested materials. This approach is of utmost importance regarding the real-life application of GO.

SEM and AFM visualization of the surface of GO papers in the initial state (deprived of thermal treatment) and GO papers annealed at 200 °C revealed two important aspects. Both CF addition into the volume of GO sheets and thermal treatment were reflected in the morphology of the resulting materials. The addition of CF increased average roughness of the GO papers, whereas thermal treatment resulted in a decrease in this parameter. Phase-contrast images revealed the biphasic internal structure of the composite papers in the initial state compared with a homogeneous structure of the pristine GO paper. An interesting outcome of this study is that regardless of the testing technique, both DMA and AFM results allowed us to state that the thermal treatment applied to the samples was followed by a decrease of their mechanical properties. We were even able to spot a bimodal distribution of the DMT modulus for the pristine GO paper that underwent thermal reduction. Yet another interesting outcome from the thermomechanical studies was related to the finding that all the investigated materials were characterized by the negative thermal expansion coefficient. It was revealed for the first time how the addition of the reinforcing material affects the GO paper thermal expansion coefficient. It was observed that even slight addition of CF significantly reduces the CTE of the investigated specimens in the pretreated state. The effective CTE of the composite material depends on the volume fractions, moduli, and CTEs of the particular composite constituents. It should be noted that CFs have a slight negative CTE in the axial direction (ca. −1*10-6 1/°C) [49] and a positive CTE in the transverse direction [50]. Because of the abovementioned CF features, the effective/resultant CTE of the CF-reinforced GO paper is significantly less negative and closer to zero than in the case of the pristine GO paper. This makes the CF-reinforced GO paper much less sensitive to temperature changes, which could be particularly important from the applicative point of view.

CRediT authorship contribution statement

Krystian Kowiorski: Methodology, Investigation, Writing – original draft, Writing – review & editing, Visualization. **Marcin Heljak:** Conceptualization, Methodology, Investigation, Writing – original draft, Writing – review & editing, Visualization. **Agata Strojny-Nędza:** Methodology, Funding acquisition. **Bartosz Bucholc:** Writing – original draft. **Marcin Chmielewski:** Writing – original draft. **Małgorzata Djas:** Conceptualization. **Kamil Kaszyca:** Formal analysis. **Rafał Zybała:** Formal analysis. **Marcin Małek:** Formal analysis. **Wojciech Swieszkowski:** Supervision. **Adrian Chlanda:** Conceptualization, Methodology, Validation, Formal analysis, Investigation, Writing – original draft, Writing – review & editing, Visualization, Supervision.

Declaration of competing interest

The authors declare that they have no known competing financial interests or personal relationships that could have appeared to influence the work reported in this paper.

Acknowledgments

This scientific work was financed as a research project “New generation thermally conductive layers for electronics and technology of their production” no. 2/Ł-IMP/CŁ/2021 financed by the Lukasiewicz Research Network (Poland).

References

[1] R. Karthick, F. Chen, Free-standing graphene paper for energy application: progress and future scenarios, Carbon N. Y. 150 (2019) 292–310, https://doi.org/10.1016/J.CARBON.2019.05.017.

[2] X. Liu, H. Zhao, X. Huang, Y. Hu, H. Gao, X. Liu, L. Shen, Fabrication of flexible graphene paper and its electrochemical properties used in lithium ion batteries, EPJ Appl. Phys. 66 (2014), https://doi.org/10.1051/epjap/2014140086.

[3] B. Nasiłowska, Z. Bogdanowicz, K. Hińcza, Z. Mierczyk, S. Góźdź, M. Djas, K. Kowiorski, A. Bombalska, A. Kowalik, Graphene oxide aerosol deposition and its influence on cancer cells, 2020, Preliminary Results, Mater 13 (2020) 4464, https://doi.org/10.3390/MA13194464, 4464. 13.

[4] K. Sałasińska, M. Leszczyńska, M. Celiński, P. Kozikowski, K. Kowiorski, L. Lipińska, Burning behaviour of rigid polyurethane foams with histidine and modified graphene oxide, Materials 14 (2021) 1184, https://doi.org/10.3390/ma14051184.

[5] J.K. Wychowaniec, J. Litowczenko, K. Tadyszak, V. Natu, C. Aparicio, B. Peplińska, M.W. Barsoum, M. Otyepka, B. Scheibe, Unique cellular network formation guided by heterostructures based on reduced graphene oxide - Ti3C2Tx MXene hydrogels, Acta Biomater. 115 (2020) 104–115, https://doi.org/10.1016/J.ACTBIO.2020.08.010.

[6] J.K. Wychowaniec, J. Litowczenko, K. Tadyszak, Fabricating versatile cell supports from nano- and micro-sized graphene oxide flakes, J. Mech. Behav. Biomed. Mater. 103 (2020) 103594, https://doi.org/10.1016/J.JMBBM.2019.103594.

[7] Ł. Kaczmarek, T. Warga, M. Makowicz, K. Kyzioł, B. Bucholc, Ł. Majchrzycki, The influence of the size and oxidation degree of graphene flakes on the process of creating 3D structures during its cross-linking, 2020, Mater 13 (2020) 681, https://doi.org/10.3390/MA13030681, 681. 13.

[8] A. Chlanda, K. Kowiorski, M. Małek, E. Kijeńska-Gawrońska, M. Bil, M. Djas, T. Strachowski, W. Swieszkowski, L. Lipińska, Morphology and chemical purity of water suspension of graphene oxide flakes aged for 14 Months in ambient conditions. A preliminary study, 2021, Mater 14 (2021) 4108, https://doi.org/10.3390/MA14154108, 4108. 14.

[9] A.R. Ranjbartoreh, B. Wang, X. Shen, G. Wang, Advanced mechanical properties of graphene paper, J. Appl. Phys. 109 (2011), https://doi.org/10.1063/1.3528213, 014306.

[10] Y. Liu, B. Xie, Z. Zhang, Q. Zheng, Z. Xu, Mechanical properties of graphene papers, J. Mech. Phys. Solid. 60 (2012) 591–605, https://doi.org/10.1016/j.jmps.2012.01.002.

[11] A.A. Muhsan, K. Lafdi, Fabrication and characterization of graphene-based paper for heat spreader applications, J. Appl. Phys. 126 (2019), https://doi.org/10.1063/1.5097000, 155109.

[12] D.A. Dikin, S. Stankovich, E.J. Zimney, R.D. Piner, G.H.B. Dommett, G. Evmenenko, S.T. Nguyen, R.S. Ruoff, Preparation and characterization of graphene oxide paper, Nature 448 (2007) 457–460, https://doi.org/10.1038/NATURE06016.

[13] B. Haiqun Chen, M.B. Mü ller, K.J. Gilmore, G.G. Wallace, D. Li, D. Li, G. G. Wallace, H. Chen, M.B. Müller, K.J. Gilmore, Mechanically strong, electrically conductive, and biocompatible graphene paper, adv, Mater 20 (2008) 3557–3561, https://doi.org/10.1002/ADMA.200800757.

[14] A. Chlanda, E. Walejewska, K. Kowiorski, M. Heljak, W. Swieszkowski, L. Lipińska, Investigation into morphological and electromechanical surface properties of reduced- graphene-oxide-loaded composite fibers for bone tissue engineering applications: a comprehensive nanoscale study using atomic force microscopy approach,, Micron 146 (2021), 103072, https://doi.org/10.1016/j.micron.2021.103072.

[15] M. Gwiazda, A. Kaushik, A. Chlanda, E. Kijeńska-Gawrońska, J. Jagiełło, K. Kowiorski, L. Lipińska, W. Święszkowski, S.K. Bhardwaj, A flexible immunosensor based on the electrochemically rGO with Au SAM using half-antibody for collagen type I sensing, Appl. Surf. Sci. Adv 9 (2022) 100258, https://doi.org/10.1016/J.APSADV.2022.100258.

[16] M. Zhang, C. Hou, A. Halder, H. Wang, Q. Chi, Graphene papers: smart architecture and specific functionalization for biomimetics, electrocatalytic sensing and energy storage, Mater. Chem. Front. 1 (2016) 37–60, https://doi.org/10.1039/C6QM00145A.

[17] L. Liu, Z. Niu, L. Zhang, W. Zhou, X. Chen, S.L. Xie Liu, Z. Niu, L. Zhang, X. Chen, W. Zhou, S. Xie, Nanostructured graphene composite papers for highly flexible and foldable supercapacitors, adv, Mater 26 (2014) 4855–4862, https://doi.org/10.1002/ADMA.201401513.

[18] M. Djas, A. Matuszewska, B. Borowa, K. Kowiorski, P. Wieczorek, M. Małek, A. Chlanda, Flake graphene as an innovative additive to grease with improved tribological properties, 2022, Mater 15 (2022) 7775, https://doi.org/10.3390/MA15217775, 7775. 15.

[19] Z.D. Huang, B. Zhang, R. Liang, Q. Bin Zheng, S.W. Oh, X.Y. Lin, N. Yousefi, J. K. Kim, Effects of reduction process and carbon nanotube content on the supercapacitive performance of flexible graphene oxide papers, Carbon N. Y. 11 (2012) 4239–4251, https://doi.org/10.1016/J.CARBON.2012.05.006.

[20] M. Nizam Uddin, Z.D. Huang, Y.W. Mai, J.K. Kim, Tensile and tearing fracture properties of graphene oxide papers intercalated with carbon nanotubes, Carbon N. Y. C (2014) 481–491, https://doi.org/10.1016/J.CARBON.2014.05.053.

[21] J. Yao, Y. Huang, Y. Hou, B. Yang, L. Lei, X. Tang, K.G. Scheckel, Z. Li, D. Wu, D. D. Dionysiou, Graphene-modified graphite paper cathode for the efficient bioelectrochemical removal of chromium, Chem. Eng. J. 405 (2021) 126545, https://doi.org/10.1016/J.CEJ.2020.126545.

[22] W. Dai, X.J. Ren, Q. Yan, S. Wang, M. Yang, L. Lv, J. Ying, L. Chen, P. Tao, L. Sun, C. Xue, J. Yu, C. Song, K. Nishimura, N. Jiang, C. Te Lin, Ultralow interfacial thermal resistance of graphene thermal interface materials with surface metal liquefaction, Nano-Micro Lett. 15 (2023) 1–14, https://doi.org/10.1007/S40820-022-00979-2/FIGURES/5.

[23] EP2842910A1-Method of Preparing Graphene Paper - Google Patents, (n.d.).

[24] Y. Yang, J. Cao, N. Wei, D. Meng, L. Wang, G. Ren, R. Yan, N. Zhang, Thermal conductivity of defective graphene oxide: a molecular dynamic study,, Molecules 24 (2019), https://doi.org/10.3390/MOLECULES24061103.

[25] X. Mu, X. Wu, T. Zhang, D.B. Go, T. Luo, Thermal transport in graphene oxide - from ballistic extreme to amorphous limit, Sci. Rep. 4 (2014), https://doi.org/10.1038/SREP03909.

[26] Y. Xie, P. Yuan, T. Wang, N. Hashemi, X. Wang, Switch on the high thermal conductivity of graphene paper, Nanoscale 8 (2016) 17581–17597, https://doi.org/10.1039/C6NR06402G.

[27] O.C. Compton, S.W. Cranford, K.W. Putz, Z. An, L.C. Brinson, M.J. Buehler, S. T. Nguyen, Tuning the mechanical properties of graphene oxide paper and its associated polymer nanocomposites by controlling cooperative intersheet hydrogen bonding, ACS Nano 6 (2012) 2008–2019, https://doi.org/10.1021/NN202928W/SUPPL_FILE/NN202928W_SI_001.PDF.

[28] N. Hu, L. Meng, R. Gao, Y. Wang, J. Chai, Z. Yang, E.S.-W. Kong, Y. Zhang, A facile route for the large scale fabrication of graphene oxide papers and their mechanical enhancement by cross-linking with glutaraldehyde, 2011, Nano-Micro Lett. 34 (3) (2011) 215–222, https://doi.org/10.1007/BF03353675.

[29] B. Wang, S. Ma, S. Yan, J. Zhu, Readily recyclable carbon fiber reinforced composites based on degradable thermosets: a review, Green Chem. 21 (2019) 5781–5796, https://doi.org/10.1039/C9GC01760G.

[30] S.M. Rangappa, S. Siengchin, J. Parameswaranpillai, M. Jawaid, T. Ozbakkaloglu, Lignocellulosic fiber reinforced composites: progress, performance, properties, applications, and future perspectives, Polym. Compos. 43 (2022) 645–691, https://doi.org/10.1002/PC.26413.

[31] Y. Su, H. Wei, R. Gao, Z. Yang, J. Zhang, Z. Zhong, Y. Zhang, Exceptional negative thermal expansion and viscoelastic properties of graphene oxide paper, Carbon N. Y. 50 (2012) 2804–2809, https://doi.org/10.1016/J.CARBON.2012.02.045.

[32] BioRender (n.d.), https://biorender.com/. (Accessed 25 January 2022).

[33] A. Cianciosi, M. Costantini, S. Bergamasco, S. Testa, E. Fornetti, J. Jaroszewicz, J. Baldi, A. Latini, E. Choińska, M. Heljak, C. Zoccali, S. Cannata, W. Święszkowski, A. Diaz Lantada, C. Gargioli, A. Barbetta, Engineering human-scale artificial bone grafts for treating critical-size bone defects, ACS Appl. Bio Mater. 2 (2019) 5077–5092, https://doi.org/10.1021/ACSABM.9B00756/SUPPL_FILE/MT9B00756_SI_004.MP4.

[34] D. Kołbuk, M. Heljak, E. Choińska, O. Urbanek, Novel 3D hybrid nanofiber scaffolds for bone regeneration, 2020, Polymer 12 (2020) 544, https://doi.org/10.3390/POLYM12030544, 544. 12.

[35] A. Chlanda, P. Oberbek, M. Heljak, Ż. Górecka, K. Czarnecka, K.-S. Chen, M. J. Woźniak, Nanohydroxyapatite adhesion to low temperature plasma modified surface of 3D-printed bone tissue engineering scaffolds - qualitative and quantitative study, Surf. Coating. Technol. 375 (2019) 637–644, https://doi.org/10.1016/J.SURFCOAT.2019.07.070.

[36] A. Nasajpour, A. Mostafavi, A. Chlanda, C. Rinoldi, S. Sharifi, M.S. Ji, M. Ye, S. J. Jonas, W. Swieszkowski, P.S. Weiss, A. Khademhosseini, A. Tamayol, Cholesteryl ester liquid crystal nanofibers for tissue engineering applications, ACS Mater. Lett. 2 (2020) 1067–1073, https://doi.org/10.1021/acsmaterialslett.0c00224.

[37] H. Ramamoorthy, K. Buapan, T. Chiawchan, K. Thamkrongart, R. Somphonsane, Exploration of the temperature-dependent correlations present in the structural, morphological and electrical properties of thermally reduced free-standing graphene oxide papers, J. Mater. Sci. 56 (2021) 15134–15150, https://doi.org/10.1007/S10853-021-06262-W/FIGURES/7.

[38] K. Thamkrongart, H. Ramamoorthy, K. Buapan, T. Chiawchan, R. Somphonsane, Investigation of the high-field transport, Joule-heating-driven conductivity improvement and low-field resistivity behaviour in lightly-reduced free-standing graphene oxide papers, J. Phys. D Appl. Phys. 55 (2022), 245103, https://doi.org/10.1088/1361-6463/AC5E19.

[39] B. Lesiak, G. Trykowski, J. Tóth, S. Biniak, L. Kövér, N. Rangam, L. Stobinski, A. Malolepszy, Chemical and structural properties of reduced graphene oxide—dependence on the reducing agent, J. Mater. Sci. 56 (2021) 3738–3754, https://doi.org/10.1007/S10853-020-05461-1/FIGURES/9.

[40] N.P. Rajkumari, S. Dolakashoria, P. Goswami, Plant-based natural dye-stimulated visible-light reduction of GO and physicochemical factors influencing the production of oxidizing species by a synthesized (rGO)/TiO2Nanocomposite for environmental remediation, ACS Omega 6 (2021) 2686–2698, https://doi.org/10.1021/ACSOMEGA.0C04889/SUPPL_FILE/AO0C04889_SI_001.P DF.

[41] G.T.T. Le, J. Manyam, P. Opaprakasit, N. Chanlek, N. Grisdanurak, P. Sreearunothai, Divergent mechanisms for thermal reduction of graphene oxide and their highly different ion affinities, Diam. Relat. Mater. 89 (2018) 246–256, https://doi.org/10.1016/J.DIAMOND.2018.09.006.

[42] O.M. Slobodian, P.M. Lytvyn, A.S. Nikolenko, V.M. Naseka, O.Y. Khyzhun, A. V. Vasin, S.V. Sevostianov, A.N. Nazarov, Low-temperature reduction of graphene oxide: electrical conductance and scanning kelvin probe force microscopy, Nanoscale Res. Lett. 13 (2018) 1–11, https://doi.org/10.1186/S11671-018-2536-Z/FIGURES/10.

[43] A. Hussein, S. Sarkar, B. Kim, Low temperature reduction of graphene oxide using hot-plate for nanocomposites applications, J. Mater. Sci. Technol. 32 (2016) 411–418, https://doi.org/10.1016/J.JMST.2016.02.001.

[44] V. Patil, R.V. Dennis, T.K. Rout, S. Banerjee, G.D. Yadav, Graphene oxide and functionalized multi walled carbon nanotubes as epoxy curing agents: a novel synthetic approach to nanocomposites containing active nanostructured fillers, RSC Adv. 4 (2014) 49264–49272, https://doi.org/10.1039/C4RA09693B.

[45] I. Zgłobicka, A. Chlanda, M. Woźniak, M. Łojkowski, R. Szoszkiewicz, M. Mazurkiewicz-Pawlicka, W. Święszkowski, E. Wyroba, K.J. Kurzydłowski, Microstructure and nanomechanical properties of single stalks from diatom *Didymosphenia geminata* and their change due to adsorption of selected metal ions, J. Phycol. 53 (2017) 880–888, https://doi.org/10.1111/jpy.12548.

[46] Ż. Górecka, J. Idaszek, D. Kołbuk, E. Choińska, A. Chlanda, W. Święszkowski, The effect of diameter of fibre on formation of hydrogen bonds and mechanical properties of 3D-printed PCL, Mater. Sci. Eng. C 114 (2020), 111072, https://doi.org/10.1016/j.msec.2020.111072.

[47] D. Attinger, C. Frankiewicz, A.R. Betz, T.M. Schutzius, R. Ganguly, A. Das, C.-J. Kim, C.M. Megaridis, Surface engineering for phase change heat transfer: a review,, MRS Energy Sustain 1 (2014), https://doi.org/10.1557/MRE.2014.9.

[48] C. Tian, Y. Xu, W.H. Kan, D. Sokaras, D. Nordlund, H. Shen, K. Chen, Y. Liu, M. Doeff, Distinct surface and bulk thermal behaviors of LiNi0.6Mn0.2Co0.2O2 cathode materials as a function of state of charge, ACS Appl. Mater. Interfaces 12 (2020) 11643–11656, https://doi.org/10.1021/ACSAMI.9B21288/SUPPL_FILE/AM9B21288_SI_001.PDF.

[49] C.-F. Yang, J.-G. Hwu, S. Min Hwang, D.-W. Kim, Y.-J. Kim, H. Mantelli, R. Alonso Martinez-Hincapie, J. Feliu, G.H. Wostenholm, B. Yates, Thermal expansion at elevated temperatures IV. Carbon-fibre composites, J. Phys. D Appl. Phys. 6 (1973) 309, https://doi.org/10.1088/0022-3727/6/3/304.

[50] E.G. Wolff, Stiffness-thermal expansion relationships in high modulus carbon fibers, 21, 81–97, https://doi.org/10.1177/002199838702100106, 2016.